

High-dimensional neural network potentials for solvation: The case of protonated water clusters in helium

Christoph Schran,¹ Felix Uhl,¹ Jörg Behler,^{2,1} and Dominik Marx¹

¹*Lehrstuhl für Theoretische Chemie, Ruhr-Universität Bochum, 44780 Bochum, Germany*

²*Universität Göttingen, Institut für Physikalische Chemie, Theoretische Chemie, Tammannstr. 6, 37077 Göttingen, Germany*

(Dated: March 25, 2021)

The design of accurate helium-solute interaction potentials for the simulation of chemically complex molecules solvated in superfluid helium has long been a cumbersome task due to the rather weak but strongly anisotropic nature of the interactions. We show that this challenge can be met by using a combination of an effective pair potential for the He-He interactions and a flexible high-dimensional neural network potential (NNP) for describing the complex interaction between helium and the solute in a pairwise additive manner. This approach yields an excellent agreement with a mean absolute deviation as small as 0.04 kJ mol^{-1} for the interaction energy between helium and both, hydronium and Zundel cations compared to CCSD(T) reference calculations with an energetically converged basis set. The construction and improvement of the potential can be performed in a highly automated way, which opens the door for applications to a variety of reactive molecules to study the effect of solvation on the solute as well as the solute-induced structuring of the solvent. Furthermore, we show that this NNP approach yields very convincing agreement with the CCSD(T) reference for properties like many-body spatial and radial distribution functions. This holds for the microsolvation of the protonated water monomer and dimer by a few helium atoms up to their solvation in bulk helium as obtained from path integral simulations at about 1 K.

Keywords: Neural Network Potentials, Quantum Solvation, Protonated Water Clusters, Superfluid Helium

I. INTRODUCTION

In recent years, helium nano droplet isolation spectroscopy¹⁻³ has proven to be a powerful method to study small molecular systems in superfluid ^4He environments which provide ultracold solvation conditions. The unique properties of this quantum fluid at temperatures in the order of one Kelvin allow one to examine solutes by means of high-resolution rotational and vibrational spectroscopy as first demonstrated in 1992.⁴ Although such low temperatures as well as the chemically inert helium environment circumvent many problems related to other experimental methods, the quantum nature of the particles is pervasive at these conditions and can not be neglected. In such situations quantum simulation techniques employing path integrals (PI) can provide reliable insight by taking the nuclear quantum effects explicitly into account.⁵ Pioneering PI simulations were able to predict the superfluid behavior of small ^4He clusters⁶ which has been confirmed experimentally ten years later.⁷ Since then a wealth of mostly Monte Carlo (MC) based studies have been performed for pure helium clusters, but also for impurities in superfluid helium or for para- H_2 clusters. Most of these studies utilize effective pair potentials for the helium-helium interaction, which have the advantage of being able to reproduce the experimental observables of pure helium under a variety of conditions with very high accuracy.⁸ In a similar spirit, also He-solute interactions are often accounted for via pairwise additive interaction potentials.⁹ This can be considered as a many-body expansion truncated after the

two-body term, which is usually acceptable since three-body terms contribute only very little as has been demonstrated by computing the three-body contributions explicitly using extrapolated CCSD(T) calculations.¹⁰ Only recently these simulation methods have been extended to also treat reactive solute species by coupling bosonic PI Monte Carlo (PIMC) simulations of helium to *ab initio* PI molecular dynamics (AI-PIMD) simulations of the solute.^{11,12}

A key component for all simulations of impurities in superfluid helium is to use a pairwise additive interaction potential between the solute and helium to be computationally efficient. The development of such potentials, however, is a rather delicate task due to the very weak interaction between helium atoms in the order of 0.1 kJ mol^{-1} (see e.g. Ref. 8) which is therefore very sensitive to small errors. To date, most of these helium-solute potentials have been specifically designed for each individual solute molecule using complicated, physically motivated functions including e.g. induction and polarization terms.^{9,10,13} The process of developing such potentials can therefore often become cumbersome and even more time consuming than the final simulations of the molecule solvated by helium.

Here, we show how machine learning techniques can be used to both, simplify and automate the task of representing the pair interaction energy between chemically complex solute molecules and helium. For this purpose we use the high-dimensional neural network (NN) methodology of Behler and Parrinello¹⁴⁻¹⁹ that has already been proven to be well suited for the description of potential energy surfaces of a variety of complex molecu-

lar systems including solvents,^{20–22} solvated ions^{23,24} and surfaces^{25,26} (for a comprehensive list see e.g. Ref. 19 and Ref. 18 where also references to alternative modern techniques are provided).

Due to the intrinsic flexibility of NNs, it is possible to easily identify atomic configurations needed for an improvement of the potential,¹⁶ which substantially reduces the number of required reference calculations compared to traditional approaches that utilize physically motivated functions.^{9,10,13} Evidently, this property greatly reduces the computational cost due to reference calculations, which might be the decisive factor if correlated and thus demanding quantum chemistry methods such as CCSD(T) shall be used. Moreover, it enables the automation of the development of interaction potentials such that the simulation of a variety of reactive molecules and complexes solvated by superfluid helium becomes feasible. In this first study along these lines, we focus on the development of two He-solute NN potentials (NNPs) for the description of hydronium (H_3O^+) and Zundel (H_5O_2^+) cations, respectively, as the two smallest protonated water clusters in the sequence of stepwise solvation of a proton by water molecules in order to shed new light on proton transfer processes in our future work.

The outline of the paper is as follows: We first describe the relevant aspects of the NN methodology and the computational details in Sec. II. The fitting procedure of the NNPs including the approach to identify relevant training configurations for improvements of the potentials are presented subsequently in Sec. III A. This is essentially a three step procedure progressing from simple sampling to importance sampling strategies to generate the training data in which we first obtain configurations of the solute molecules as the basis for the generation of He-solute pairs. In a second step, the properties of the NNs are used to iteratively target He-solute pairs needed for an improvement of the interaction potential, thus providing a powerful tool to reduce the number of expensive reference calculations. Afterwards, the NNPs are applied in full path integral quantum simulations including many solvent He atoms to generate, detect and incorporate those solvation structures that are not already covered by the included He-solute pairs. Finally, the converged pairwise additive He-solute NNPs are applied to simulate helium around selected fixed solute configurations starting with microsolvation up to the helium bulk phase, see Sec. III B and III C, in order to assess the quality of the developed potentials, followed by conclusions and outlook.

II. METHODS

A. Determination of the Training and Test Configurations

To generate reference structures of the solute molecules similar to the configurations in superfluid helium, we performed density functional theory based AI-PIMD simu-

lations²⁷ of the bare solute cations H_3O^+ and H_5O_2^+ in vacuum but at the same ultralow temperature. This approach is justified since it is known that He-solvation has only a minor effect on solute structure.³ These simulations have been carried out with our in-house developer’s version of the CP2k program package^{28,29} in a 9.0 Å cubic box with cluster (i.e. non-periodic) boundary conditions. The electronic structure in the AI-PIMD simulations was solved on-the-fly using the Quickstep module³⁰ by applying the RPBE exchange correlation functional³¹ together with the D3 dispersion correction³² up to two-body terms. The charge density was represented on a grid up to a plane wave cutoff of 500 Ry. The TZV2P basis set together with Goedecker-Teter-Hutter pseudopotentials to replace the core electrons in the oxygen atoms³³ was used for the description of the Kohn-Sham orbitals. The SCF cycles were converged to an error of $\epsilon_{\text{SCF}} = 10^{-7}$ Ha. This electronic structure setup is known to reproduce many properties of water in good agreement with experiment.^{20,34,35} For each solute molecule 27.5 ps AI-PIMD trajectories were generated with a time step of 0.25 fs at a temperature of 1.67 K where the path integral has been discretized in terms of 48 replicas. The PIGLET algorithm³⁶ recently extended to ultralow temperatures³⁷ was applied to sample the canonical quantum distribution. At the beginning of each trajectory, 2.5 ps have been discarded as equilibration starting from the optimized minimum energy configuration.

From these reference ensembles we extracted structures for the hydronium and Zundel cations with a time lag of 25 fs from all 48 PI replicas, resulting in 48 000 uncorrelated path integral quantum configurations. These structures have been used as the basis for the generation of helium sample positions as described later in detail, thus producing a large ensemble of He-solute pair configurations for the following reference electronic structure calculations. Note that we restrict the interaction potentials to He-solute two-body interactions, since higher-order many-body terms have recently been shown to be negligible.¹⁰ The He-solute interaction energies were calculated within the usual supermolecule approach via CCSD(T), being broadly considered to be the “gold standard” of quantum chemistry, employing the aug-cc-pVTZ basis set^{38,39} with a counterpoise correction⁴⁰ to correct for the basis set superposition error, dubbed AVTZcp in the following. This electronic structure setup is shown to produce negligible remaining basis set errors compared to the complete basis set limit as presented in Section I A of the SI. All interaction energy calculations for the He-solute structures were performed with the Molpro program package.⁴¹

B. Neural Network Fitting

The construction of the NNPs for the description of the helium-solute interaction energies is achieved by fol-

lowing a similar procedure as established by Behler and coworkers.^{14,16} However, instead of the total energy of the system as before, the He-solute interaction energy is used as target for the fit. The two-body interaction energy E^{int} in any specific He-solute configuration is then calculated as in the realm of conventional high-dimensional NNPs from atomic contributions E_i^{NN} for which independent atomic NNs are fitted,

$$E^{\text{int}} = \sum_i^{N_{\text{atom}}} E_i^{\text{NN}} , \quad (1)$$

where N_{atom} denotes the number of atoms in the system. In order to construct the analytic structure-atomic energy relation, first the atomic coordinates of the system are transformed to sets of many-body atom-centered radial and angular symmetry functions⁴² as usual, which serve as input vectors for the atomic NNs. This ensures the required invariances of the energy with respect to translations and rotations of the system as well as to permutations of atoms of the same element. For both types of symmetry functions employed here, a cutoff function

$$f_c(R_{ij}) = \begin{cases} 0.5 \cdot \left[\cos\left(\frac{\pi R_{ij}}{R_c}\right) + 1 \right] & \text{for } R_{ij} \leq R_c \\ 0 & \text{else} \end{cases} \quad (2)$$

depending on the distance R_{ij} between the central atom i and a neighboring atom j is used to define the atomic environment up to a certain cutoff radius R_c . The radial arrangement of the atoms within this cutoff sphere is accounted for by a product of a Gaussian and the cutoff function according to Eq. (2),

$$G_i^2 = \sum_j e^{-\eta(R_{ij}-R_s)^2} \cdot f_c(R_{ij}) , \quad (3)$$

where different regions around the central atom i can be probed by adapting the width of the Gaussian η and the shifting parameter R_s . To complement the description of the environment around each atom, angular functions of the form

$$G_i^4 = 2^{1-\zeta} \sum_{j,k \neq i, j \neq k} (1 + \lambda \cos \theta_{ijk})^\zeta \cdot e^{-\eta(R_{ij}^2 + R_{ik}^2 + R_{jk}^2)} \cdot f_c(R_{ij}) \cdot f_c(R_{ik}) \cdot f_c(R_{jk}) \quad (4)$$

are employed that depend on the angle θ_{ijk} between the central atom i and two neighbors j and k , where i, j and k can be any atom of the He-solute complex. Different angular regions are probed by adjusting the exponent ζ . The parameter λ , which can have values of $+1$ or -1 , is used to shift the maximum of the cosine either to π or 2π .

A set of these symmetry functions for each element, as specified in Section I.D of the SI, transforms the coordinates of the system to be employed as input for the NN. We finally selected different sets for the He-hydronium and He-Zundel interaction potentials in order to reduce

the number of symmetry functions to a minimum. For He-hydronium we employed 60 such functions, while 79 are used for the He-Zundel NNP. The values of each symmetry function are furthermore centered around the average value of the training set and normalized to values between zero and one following the usual procedure.

These vectors serve as the input for the atomic NNs, which consist in all cases of two hidden layers with 25 nodes each, and yield the atomic energy contributions that sum up to the total interaction energy. Bias nodes with weight parameters b were attached to all layers but the input layer. Note that the evaluation of a NN node value y is essentially a linear transformation of the values of the previous layer y_i by the associated weight parameters a_i , that is further transformed by a non-linear activation function f

$$y = f \left(b + \sum_{\text{previous}}^{\text{layer}} y_i \cdot a_i \right) . \quad (5)$$

We used the hyperbolic tangent in all hidden layers and a linear activation function for the output layer in order to prevent a confined range of output values.

The NNPs are constructed by first splitting the set of CCSD(T) reference data into a training set (90%) and an independent test set (10%) of He-solute configurations. Subsequently, the weight parameters of the NNs are iteratively optimized to minimize the error of the training set, while the test set provides an estimate for the transferability to structures not included in the training set and is used to detect over fitting. Learning was achieved by optimizing the weights a and b according to the adaptive global extended Kalman filter⁴³⁻⁴⁵ as implemented in our in-house program `RunNER`.⁴⁶

C. Path Integral Simulations

In order to incorporate the solvation effect on the solute structure and to use NNPs in (ab initio) path integral simulations, the NNs have been implemented in our in-house version of the `CP2k` program package²⁸ to provide energies and forces for the hybrid PIMD / bosonic PIMC technique.^{11,12}

To identify solute configurations outside the structural range of the vacuum ensemble formed by helium-solute pairs, which might emerge during helium solvation, we conducted short 10 ps AI-PIMD/PIMC simulations^{11,12} of the fully flexible solutes in bulk helium starting from equilibrated vacuum solute configurations and coupling the solutes to the helium environment via the NNPs. The solutes were simulated together with 98 and 88 helium atoms for the H_3O^+ and H_5O_2^+ cation, respectively, in a truncated octahedron cell with periodic boundary conditions and a distance between the parallel square faces of 19.117 Å. The number of helium atoms placed in this box were chosen according to a comparison of radial distribution functions (RDFs) as presented in Section I.C of

the SI. Helium was treated using the pair density matrix approximation⁵ together with the Aziz He-He pair interaction potential.⁸ The temperature was set to 1.67 K and the high-temperature pair density matrix at 80 K was used together with 48 beads in order to discretize the low-temperature density matrix at 1.67 K. The solute was described by the same setup as for the vacuum simulations presented in Sec. II A. Following our earlier work on the solvation of molecules in superfluid helium,^{11,12} the He-solute interactions are discretized using the primitive approximation whereas the development of higher-order actions involving NNP couplings are a subject of future research. In between any two AI-PIMD steps, 10 000 PIMC steps were performed to ensure sufficient helium sampling according to the LaBerge-Tully “MDMC algorithm”.⁴⁷

In order to validate the quality of our two final NNPs compared to CCSD(T)/AVTZcp data, we evaluated the interaction potential of five frozen structures of the target solutes on a cubic grid. Bulk helium and helium microsolvation can be simulated surrounding the clamped solute structures by evaluating the solute-helium interaction on the grid using the nearest neighbor approach, thus assigning the interaction in continuous space to the nearest grid point. The structures were centered in a cubic grid with 50 grid points in each dimension and a grid spacing of 0.25 Å. This results in 125 000 CCSD(T) calculations for each structure that are not used in the fitting process, but only for the validation of the potentials. It should be noted that this rigorous “real life” validation step requires one order of magnitude more calculations than the actual NNP fitting procedure, and is used here exclusively to demonstrate the power of the proposed approach as proof of concept.

Subsequent helium PIMC simulations were performed with the same settings as for the flexible solute simulations, but involved 20 PIMC walkers with randomized helium starting configurations and different random number seeds for bulk helium. Each walker generated 1 000 000 structures with 1000 PIMC steps in between to guarantee uncorrelated configurations. Microsolvation was simulated for 1, 2, 4, 6, 10 and 14 helium atoms with 100 PIMC walkers in a 15 Å droplet radius and otherwise using the same settings as for the bulk. To estimate if the simulation length is sufficient, we compared spatial properties for a selected configuration obtained with the described settings to those resulting from ten times improved statistics as presented in Sec. II.C of the SI. Since these observables are essentially the same, it can be concluded that the here reported properties are statistically converged. Bosonic helium exchange^{11,12} was disabled for all calculations to increase the sampling efficiency.

III. RESULTS AND DISCUSSION

A. Automated Neural Network Fitting Procedure and Iterative Improvement

In order to describe the interaction potential between protonated water clusters and helium, we developed the following procedure to select relevant configurations for the training of the NNP. We started by using converged ensembles of the solutes in vacuum obtained as described in Sec. II A as the basis for the generation of helium sample positions. This is based on the assumption that helium solvation has only a small effect on the solute structure and will be accounted for in a subsequent step. In contrast to interaction potentials based on physical principles, it is not sufficient to use only stationary points on the potential energy surface of the solutes since NNs are not able to extrapolate. Therefore, the whole range of possible configurations must be represented by the training set in contrast to traditional approaches to generate helium-solute pair potentials.^{10,13} However, to restrict the reference calculations to the relevant parts of configuration space, we used a simple sampling MC scheme on atom centered grids around the solute atoms. Helium configurations very close to the solute molecule are very high in energy due to Pauli repulsion. We therefore determined a lower cutoff radius around each atom type by analyzing a radial scan for the minimum energy structures of the He-H₃O⁺ adduct. We afterwards restricted our atom centered grids to helium positions with distances exceeding 2.05 Å for oxygen and 1.25 Å for hydrogen atoms. A detailed discussion of the radial scan can be found in Section I.B of the SI. Moreover, configurations far away from the solute feature very small and slowly changing interaction energies and thus this region does not need to be sampled as extensively as the region closer to the solute. We therefore applied Euler-Maclaurin radial grids⁴⁸ with $N_{\text{rad}} = 25$ points which use smaller intervals close to the center. Helium configurations farther away than 10.0 Å were excluded explicitly, since they exhibit interaction energies smaller than 0.01 kJ mol⁻¹ and are usually outside the range encountered in our envisaged helium bulk simulations. This consideration results in the following interatomic distance constraints

$$r_{\text{X-He}} = \begin{cases} 2.05 \text{ \AA} < r_{\text{O-He}} < 10.0 \text{ \AA} \\ 1.25 \text{ \AA} < r_{\text{H-He}} < 10.0 \text{ \AA} \end{cases} \quad (6)$$

for possible helium configurations around the solute ensembles.

For each distance on the Euler-Maclaurin radial grid we generated $N_{\text{ang}} = 110$ additional angular points using the Lebedev quadrature formula⁴⁹ and each shell was rotated around a random axis by a random angle. This product of radial and angular grids centered around each solute atom of every solute configuration extracted from the vacuum reference simulations results in roughly $N_{\text{sol. struc.}} \cdot N_{\text{sol. atoms}} \cdot N_{\text{rad}} \cdot N_{\text{ang}}$ He-solute structures,

some of which are excluded due to the lower and upper cutoff according to Eq. (6). On this large ensemble of structures, we performed MC simple sampling to extract He-solute configurations for H_3O^+ and H_5O_2^+ . With this procedure only 1000 statistically independent helium-solute configurations were generated as the reference set for the first stage of our NNP generation protocol.

Due to the flexibility of NNs, energy predictions of two distinct NNPs vary considerably for structures differing significantly from the training configurations.¹⁶ This allows us to identify most efficiently configurations that are needed for an improvement of the NNP without performing computationally demanding CCSD(T) calculations for the identification of these points. To systematically extend the reference set we therefore developed the following strategy. In each refining stage, additional 100 000 He-solute configurations for both solutes were generated by the same procedure as before with slight modifications. Structures in the Pauli repulsion regime and in the interaction well feature larger absolute interaction energies than structures farther away from the solute molecule. The resulting absolute difference between two NNPs is thus also larger compared to interaction energies close to zero (assuming that the prediction is not completely unreasonable). As before, we randomly selected 1000 structures of the solute vacuum ensemble as the basis for helium sampling positions. However, to circumvent a biased selection of structures in the interaction wells and in the Pauli repulsion dominated region, we afterwards randomly selected one of the following three intervals for the radial grids around each solute atom to systematically improve different regions of the interaction potential, namely

$$\begin{aligned} r_{\text{X-He}}^1 &= \begin{cases} 2.05 \text{ \AA} < r_{\text{O-He}} < 10.0 \text{ \AA} \\ 1.25 \text{ \AA} < r_{\text{H-He}} < 10.0 \text{ \AA} \end{cases} \\ r_{\text{X-He}}^2 &= \begin{cases} 2.5 \text{ \AA} < r_{\text{O-He}} < 10.0 \text{ \AA} \\ 1.5 \text{ \AA} < r_{\text{H-He}} < 10.0 \text{ \AA} \end{cases} \\ r_{\text{X-He}}^3 &= \begin{cases} 4.0 \text{ \AA} < r_{\text{O-He}} < 10.0 \text{ \AA} \\ 3.0 \text{ \AA} < r_{\text{H-He}} < 10.0 \text{ \AA} \end{cases} \end{aligned} \quad (7)$$

The two additional cutoffs are chosen according to the first and second coordination shell around the solutes. Afterwards, we evaluated the interaction energies for the set of additional configurations with two different NNPs and extracted the 1000 structures with the highest energy differences. For each of these configurations we performed CCSD(T) reference calculations and the new data was then combined with the old CCSD(T) data set to serve as input for the fit of the refined NNPs at the next stage. This procedure allows us to systematically improve the NNPs, while substantially lowering the number of expensive CCSD(T) reference calculations. Overall, we iteratively improved the NNP for He-hydronium in 12 such refinement stages, while 21 stages were used for the He-Zundel NNP to account for the larger number of

degrees of freedom. We thus used only 12 000 and 21 000 reference CCSD(T) calculations for the hydronium and Zundel complex, respectively.

In a next step we explicitly incorporated the solvation effect of helium on the solute structure by conducting short AI-PIMD/PIMC simulations of the two fully flexible solutes in bulk helium coupled via the refined NNPs as described in detail in Sec. II C. During these simulations, we are able to identify structures that are missing in our training set by comparing the encountered symmetry function values to the range of values in the training set. Structures outside the range are extrapolating and therefore have to be included for a reliable NN description of the interaction energy. During the short simulations that already evaluate the NNP many million times, we identified and extracted 3545 and 4101 structures that feature symmetry function values outside the range of the training set for the H_3O^+ and H_5O_2^+ molecule, respectively, and performed reference CCSD(T) calculations for all of them. They were afterwards combined with the previous training sets to parameterize the final interaction potentials.

The correlation between the reference CCSD(T)/AVTZcp energies and the NNP interaction potential of the final training and test sets is shown in Fig. 1. For both solutes almost perfect correlation is achieved for the training as well as the test set over the whole range of interaction energies. The Zundel cation features overall smaller helium interaction energies than the hydronium cation. The strongest interaction for He-hydronium in the reference set is $-5.77 \text{ kJ mol}^{-1}$, while for He-Zundel it is only $-3.35 \text{ kJ mol}^{-1}$. This is due to a larger charge localization in the smaller H_3O^+ species that therefore results in stronger interaction with helium. The lower panels of the figure additionally show the deviation of the predicted energies over the whole range of the reference set. These are consistently small, with slightly larger deviations in the repulsive regime which, however, also features one order of magnitude larger energies. The mean absolute differences (H_3O^+ : $0.023 \text{ kJ mol}^{-1}$ training set, $0.035 \text{ kJ mol}^{-1}$ test set; H_5O_2^+ : $0.030 \text{ kJ mol}^{-1}$ training set, $0.041 \text{ kJ mol}^{-1}$ test set) are of comparable order in the training and test set as well as for both networks. These values are considerably lower than for other interaction potentials that have been obtained in a traditional fitting approach to physically derived He-solute interaction potentials of other systems.^{10,13} In addition, as shown in the insets of the upper panels of Fig. 1, the histograms over the deviations of the predicted energies for the training and test set are very narrow with standard deviations in the order of 0.05 kJ mol^{-1} and thus well below the He-He interaction of 0.1 kJ mol^{-1} . It can therefore be concluded that NNs are able to fit interaction energies with very high precision. In addition, our presented method of selecting reference configurations allows for fast improvement of the interaction potentials and substantially reduces the number of computationally de-

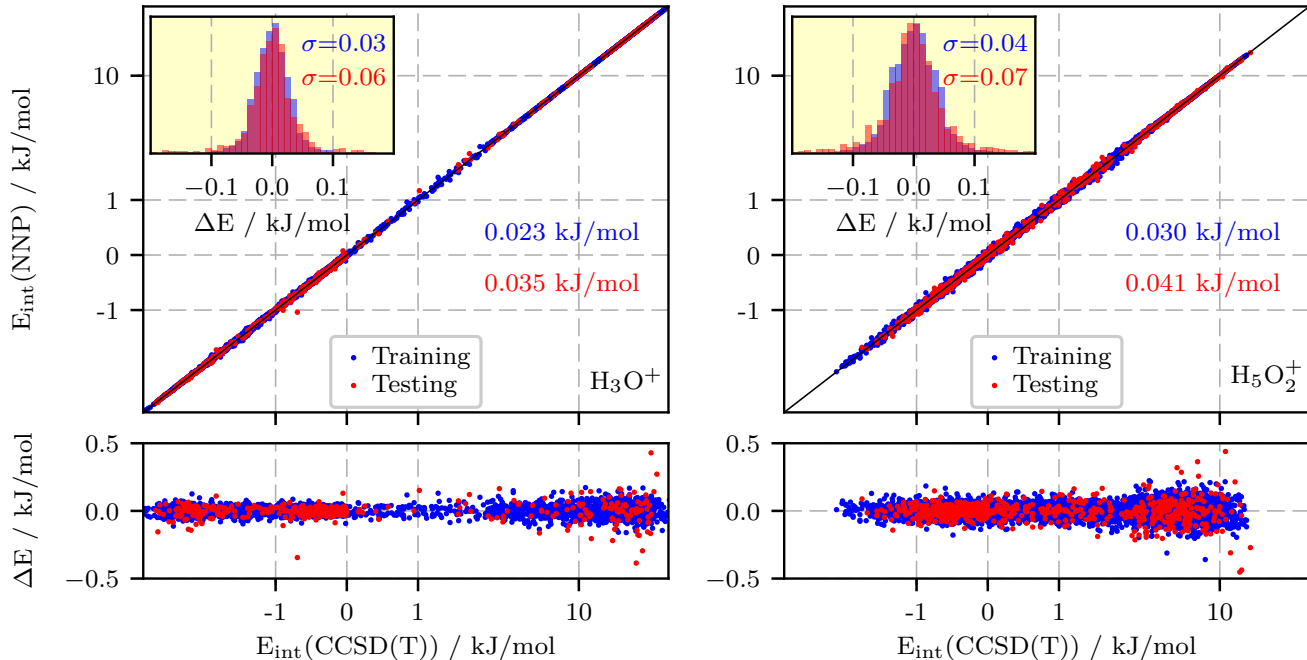


Figure 1. Correlation of the interaction energy from explicit CCSD(T)/AVTZcp calculations and NNP prediction for the final reference data set, see text. Results for the He-hydronium (H_3O^+) interaction potential are shown in the left panel, while the results of the He-Zundel (H_5O_2^+) interaction potential are depicted in the right panel. The mean absolute difference for the training and test set are depicted in blue and red, respectively. The lower two panels show the energy differences between coupled cluster reference and NNP prediction over the whole range of reference energies, while the insets show the histograms over the energy differences including the corresponding standard deviations σ in the respective color which are well below the He-He interaction energy.

manding CCSD(T) calculations compared to traditional approaches.^{10,13} Finally, we stress that the protocol developed for hydronium and Zundel cations can be readily automated and thus generalized to other solutes in helium.

B. Helium Microsolvation

The canonical way to evaluate the quality of NNPs is to compare to calculations performed with the method used to determine the reference data set. In our case this would imply to run our envisaged hybrid AI-PIMD/PIMC quantum simulation and evaluate the CCSD(T) energy in each and every AI-PIMD and PIMC step as well as the forces in every AI-PIMD step of the simulation. Unfortunately, this method is out of scope, since one MC cycle requires already around 40 million (number of helium atoms N_{He} times number of path integral replica N_{Rep} times number of auxiliary MC steps N_{MC}) evaluations of the interaction energy. Note that it is of course possible to compare radial scans around selected solute structures as demonstrated for the hydronium cation in Section I.B of the SI. However, this approach examines only a very small fraction of the full

configuration space and does not incorporate the influence of He-He interactions.

In order to meaningfully validate the quality of the converged NNPs, we recourse to the approach established in Ref. 10. For a selected set of relevant fixed structures of the solute the evaluation of the interaction potential on a grid is still feasible even using the demanding CCSD(T)/AVTZcp reference method. Afterwards, helium can be simulated surrounding the clamped solute structures by evaluating the solute-helium interaction on the grid using the nearest neighbor approach in addition to the usual He-He pair interactions.⁸ This is significantly faster than the evaluation of the NNP in continuum space by three orders of magnitude. However, evaluating the NNPs takes on the order of 0.1 ms on a single core, while the CCSD(T) reference calculation needs 60 s for H_3O^+ and 22 min for H_5O_2^+ ; all reported timings were obtained on an Intel(R) Xeon(R) CPU E5-2630 v4 @ 2.20GHz. Density functional theory calculations as described in section II A, which might be used as an alternative method to determine the interaction energy on-the-fly, require 6 s for H_3O^+ and 50 s for H_5O_2^+ on a single core. To estimate the influence of this grid-based approach on the helium solvation structure, simulations using the NNP in continuum space can be conducted.

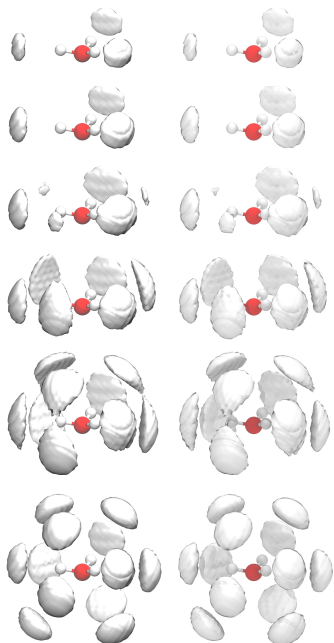


Figure 2. Comparison of helium SDFs, see text, obtained from path integral simulations with (from top to bottom) 1, 2, 4, 6, 10 and 14 helium atoms in the field of a frozen H_3O^+ configuration close to its minimum energy structure ('Minimum'). Left: Energies obtained from the coupled cluster grid. Right: NNP evaluated at the coupled cluster grid points. The isovalue is set to $0.2 \cdot 10^{-3} \text{ 1/bohr}^3$ in all shown cases.

For this procedure we chose two structures from the vacuum reference ensemble of the H_3O^+ molecule. The first one is close to the minimum energy configuration with slight deviations in the O-H bond length and will be abbreviated as 'Minimum', while the second one is a planar structure close to the transition state of the pseudo rotation and is called 'Flat'. For the H_5O_2^+ molecule three structures were selected from the reference ensemble. The first is again closely related to the minimum energy structure ('Minimum'), the second one is a planar structure ('Flat') and in the third one the proton is in a very asymmetric position ('Asymm'). The interaction potential of these structures was evaluated as described in Sec. II C and afterwards applied to study microsolvation of the solute by different numbers of helium atoms in the first step. As a key property to compare the reference and NNP grid, we chose to calculate the spatial distribution function (SDF) of helium, since it is highly sensitive to small changes in the interaction energies. The integral over space was normalized to the number of helium atoms in order to compare the SDFs with different numbers of helium atoms at the same isosurface value.

The comparison of the reference and the NNP grid of hydronium microsolvated by helium is depicted in Fig. 2 for the Minimum configuration. Overall, there are no noteworthy deviations between the SDFs of the reference and the neural network for all shown numbers of helium atoms. Therefore, in the following we present the struc-

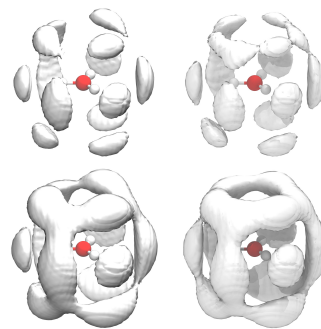


Figure 3. Comparison of helium SDFs obtained from path integral simulations with 14 helium atoms in the field of a frozen H_3O^+ configuration in a flat orientation ('Flat'). Left: Energies obtained from the coupled cluster grid. Right: NNP evaluated at the coupled cluster grid points. Top: isovalue = $0.2 \cdot 10^{-3} \text{ 1/bohr}^3$. Bottom: isovalue = $0.08 \cdot 10^{-3} \text{ 1/bohr}^3$; note that the SDFs have been normalized to the number of helium atoms.

tural changes upon increasing helium microsolvation of both grids combined.

Microsolvation with one helium atom results in trapping the helium atom inside one of the interaction wells that are located about 2 \AA away from the hydrogen atoms in the direction of the O-H bonds. During the simulations we did not observe hops between the three almost equally deep wells and the appearance of three volumes of accumulated density (VAD) is only a result of sampling with multiple MC walkers with different random number seeds in agreement with previous findings.¹⁰ The SDFs of two and three (not shown) helium atoms are therefore almost identical to those with one atom. When a fourth helium is added, however, it populates one of the three spatial regions in between two interaction wells in order to maximize its helium-helium interactions. Again, the VADs appear in all three possible positions only due to averaging over independent MC walkers. For five (not shown) and six helium atoms these positions are saturated stepwise. Addition of further helium atoms extends the solvation to the region on top of the hydronium cation (in our chosen reference frame as depicted in Fig. 2) as shown for ten helium atoms. This region still features attractive interaction energies and is in closer proximity to the hydrogen atoms than to the oxygen atom. The helium atoms in between the interaction wells are pushed slightly out of the direct connection of the wells and as a result, the VADs in the wells are elongated in the perpendicular direction to the oxygen-hydrogen bonds in order to increase the helium-helium interaction. Microsolvation with 14 helium atoms results in a closed first hydration shell also in the region closer to the oxygen atom that features smaller interaction energies. As already stated, the two grids yield almost identical SDFs for all studied numbers of helium atoms and it can therefore be concluded that the NNP describes the microsolvation of this hydronium configuration quantitatively compared to the

CCSD(T)/AVTZcp reference.

For the sake of clarity, we do not present this comparison for all selected solute structures, since their general dependence on the number of helium atoms is similar and the results obtained with the NNP grids are very close to the reference in most cases. Instead, we present all helium SDFs in Section II of the SI and concentrate here on situations where we do not observe perfect agreement between the reference and the NNP. The first of these cases is the microsolvation of the flat hydronium structure by 14 helium atoms as depicted in Fig. 3. Although up to this number of helium atoms we observe again very good agreement between the two grids as can be seen in Sec. II.A in the SI, the shown SDFs feature small differences. The region in between the upper VADs for the larger isovalue depicted in the figure is connected for the NNP grid, while it is not for the reference grid. However, this is merely a consequence of the high sensitivity to the isovalue chosen to represent the SDFs. For smaller isovalues this connection also appears for the reference grid and the differences between the grids are again very small as shown in the lower panel of Fig. 3. This thus suggests that the NNP energy is slightly too shallow in this particular region of the interaction potential. Note that these findings are converged with respect to the simulation length as presented in Sec. II.C of the SI where we compare the SDFs to simulations with ten times improved statistics. In addition, flat hydronium structures like the one used for the grid are very rare and make up only 3 % of the vacuum reference ensemble. We are therefore confident that this small difference in relative energies is of minor importance for the overall microsolvation of H_3O^+ by helium.

Microsolvation of the Zundel cation by helium is equally well described by the NNP for almost all numbers of helium atoms that have been studied for the three selected H_5O_2^+ structures. The reader is again referred to the SI, see Section II.A therein, for a comprehensive comparison. Again, we only present here the two cases where the SDFs obtained on the NNP grid apparently deviate from the reference as depicted in Fig 4. Actually, the selected H_5O_2^+ configuration with asymmetric proton sharing is the only candidate where the SDFs of the NNP grid and the reference grid partially disagree, specifically for four and 14 helium atoms. While the reference grid for $n = 4$ helium atoms provides two VADs in between the VADs of the interaction wells as visible at the larger isovalue in Fig 4 on the side of the hydronium-like motif of the complex, the minima on the NNP are too close and therefore displace the remaining two helium atoms to the surrounding. In addition, the part of the interaction potential around the excess proton is shallower on the NNP grid, similarly as observed for the flat H_3O^+ configuration. This results in connected VADs in the case of microsolvation with 14 helium atoms, although the position of the remaining VADs is well captured by the NNP. The discrepancies are again eliminated when the SDFs are visualized at smaller isovalues as shown in

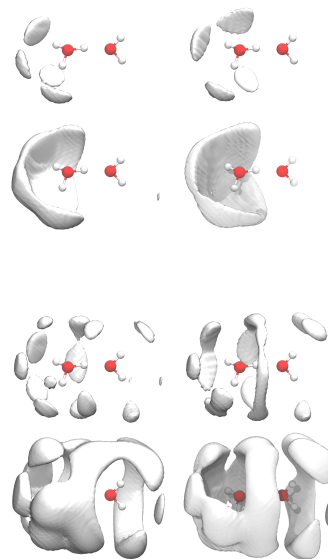


Figure 4. Comparison of helium SDFs obtained from path-integral simulations with 4 (two top panels) and 14 (two bottom panels) helium atoms in the field of a frozen H_5O_2^+ configuration in an asymmetric proton transfer situation ('Asymm'). Note that configuration with a similar value of the proton transfer coordinate only make up for around 1-2 % of all configurations. Left: Energies obtained from the coupled cluster grid. Right: NNP evaluated at the coupled cluster grid points. The isovalue for both numbers of helium atoms in the upper representation was set to $0.2 \cdot 10^{-3} \text{ 1/bohr}^3$, while for the lower representation it was set to $0.035 \cdot 10^{-3} \text{ 1/bohr}^3$; note that the SDFs have been normalized to the number of helium atoms.

Fig 4 which gives us confidence that the microsolvation of this species is essentially described correctly by the NNP. In addition, the excess proton in this configuration features a comparable O-H bond length as for the dangling hydrogen and is, thus, in an unfavorable configuration. Actually, structures with a similar proton sharing situation only account for 1-2% of the vacuum ensemble and are therefore again of minor importance. We therefore conclude that also the microsolvation of the Zundel cation by helium is captured correctly by the converged NNP.

C. Bulk Helium Solvation

In order to probe the quality of the developed NNPs for solvation of these protonated water clusters in bulk helium, we performed bulk simulations using the same nearest neighbor approach as employed in the previous section which is described in detail in Sec. II.C. In addition to the SDFs, we also chose to calculate the RDFs between the solute atoms and helium as defined in Ref. 50, since they provide easier insight into the solute-induced structuring of the solvent in terms of the different solvation shells. The oxygen- and hydrogen-helium RDFs of

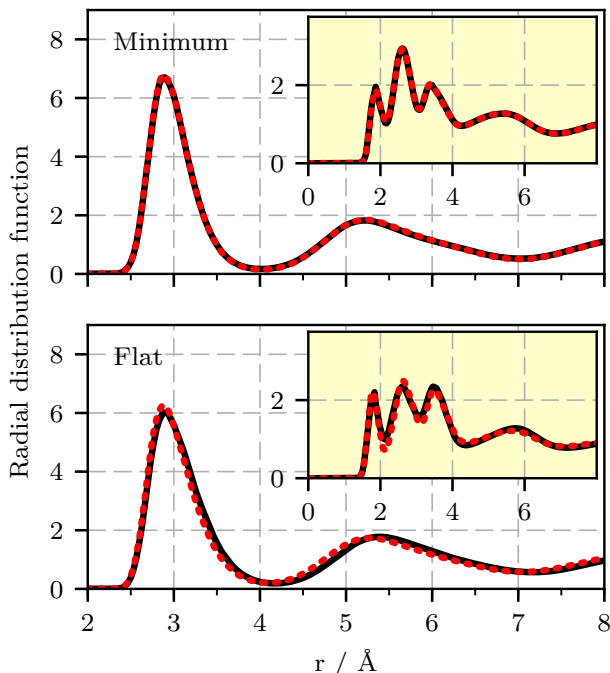


Figure 5. Radial distribution function for oxygen-helium (main) and hydrogen-helium (inset) for frozen H_3O^+ configurations in bulk helium in a selected orientation close to the minimum energy structure (‘Minimum’, top) and in a flat orientation (‘Flat’, bottom) centered in a truncated octahedron periodic supercell hosting in addition 98 He atoms. Black, solid: Energies obtained from the coupled cluster grid. Red, dotted: NNP evaluated at the coupled cluster grid points.

the H_3O^+ molecule in bulk helium are shown in Fig. 5 for both reference structures, Minimum and Flat. Note that we present only one representative H-He RDF for both reference structures, namely in both cases the RDF of the left hydrogen atom defined according to the reference frame in Figs. 2 and 3. The other RDFs are very similar and feature the same agreement between NNP and CCSD(T) grid.

The first helium solvation shell has its maximum at roughly 2.9 Å apart from the oxygen atom for both structures, while the second shell peaks at 5.3 Å. In between the two peaks the O-He RDFs decay almost to zero, suggesting that the first solvation shell is very well structured and that helium atoms do not migrate much between the shells. This conclusion is also supported by the sharp and intense peak of the first shell and is consistent with the anisotropic helium distributions around solutes from earlier predictions in pioneering studies on this subject using very simple He-solute interaction models.^{51,52} It is also consistent with the general notion of “frozen” helium atoms that are tightly bound to certain impurities.^{53–56} The fine structure of the first shell can be better seen in the H-He RDFs shown in the inset of the figure for one of the hydrogen atoms. They feature three pronounced

peaks in line with the well structured VADs observed for the microsolvated solute configurations. As in the previous section, the NNP grids yield almost identical RDFs compared to the reference CCSD(T) grid for both structures. In case of the flat configuration that accounts only for 3% of the ensemble, there are small deviations, but the overall bulk solvation pattern according to the reference grid is reproduced very well by the NNP. Note that the observed differences are in the same order than the basis set error introduced by not using the complete basis set limit as shown in Section I.A of the SI.

As expected from the RDFs, the SDFs of the structure close to the minimum energy configuration are in perfect agreement (only shown in Section II.B of the SI) and compare in their first solvation shell well with the microsolvation shell obtained with 14 helium atoms. The SDFs of the flat configuration (shown in Section II.B of the SI), feature small deviations that can again be explained by similar reasons as before: Some parts of the interaction potential are slightly shallower on the NNP grid and thus yield pronounced VADs already at higher isovalues compared to the reference grid. The same arguments as presented in the previous section in combination with the good agreement of the RDFs gives us confidence that the solvation by bulk helium of even rare event structures like the flat configuration, being close to the transition state of the pseudorotation of the H_3O^+ cation, is correctly described by our He-hydronium NNP.

Finally, let us focus on the H_5O_2^+ cation and its solvation by bulk helium. The comparison of the O-He and H-He RDFs for the three selected configurations is depicted in Fig. 6. As before, we present only two representative RDFs for each reference structure, namely the H-He RDF of the shared proton for Minimum and the H-He RDFs of a selected dangling hydrogen for Flat and Asymm. The O-He RDFs are shown for the left oxygen atom according to the reference frame in Fig. 4 and Sec. II.A of the SI. Again, the other RDFs are similar and yield the same level of agreement between NNP and CCSD(T) grid. Compared to the H_3O^+ molecule, the first O-He shell peaks at larger distances of about 3.2–3.4 Å and are also broader. This implies a less tight binding in the first solvation shell compared to the hydronium cation which is supported by the higher probability at the first minimum in the RDFs compared to the H_3O^+ molecule. Also our findings from Sec. III A that the maximum of the interaction potential between helium and the Zundel cation is about 2.5 kJ mol⁻¹ lower is in accordance with these less structured RDFs. As expected, the sharpest first peak is observed for the structure with an asymmetric proton which features the largest charge localization. As already found for the smaller H_3O^+ molecule, the NNP grids provide almost identical RDFs compared to the reference grids for all three selected structures. Also the SDFs of H_5O_2^+ in bulk helium support the conclusion that the NNP is able to describe the helium-solute interaction with almost perfect agreement to the reference as can be seen in Section II.B of the SI. Even for the con-

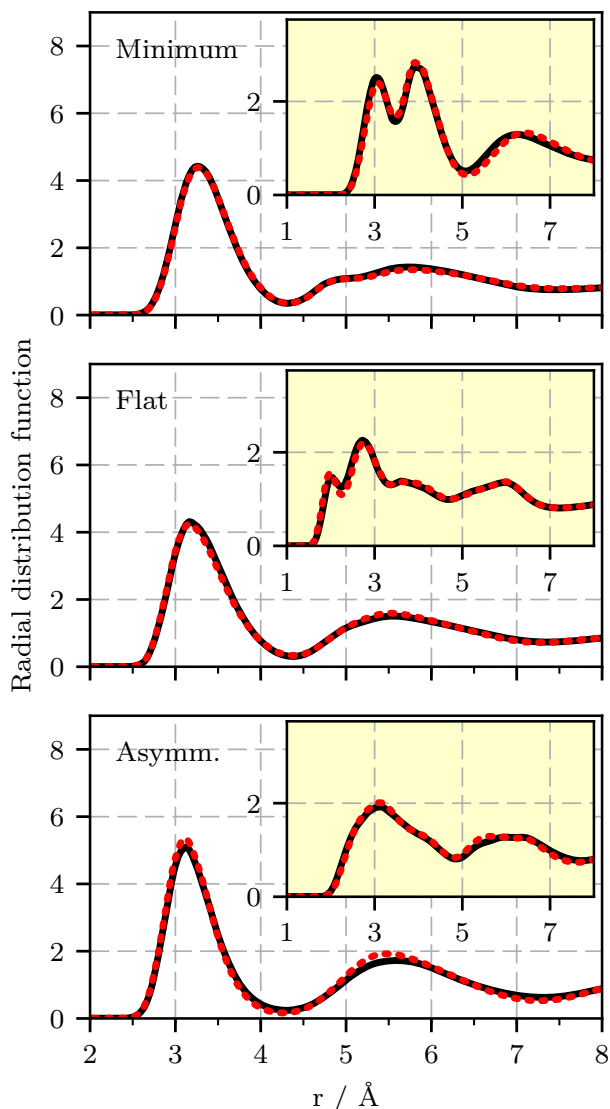


Figure 6. Radial distribution function for oxygen-helium (main) and hydrogen-helium (inset) for frozen H_5O_2^+ configurations in bulk helium in a selected orientation close to the minimum energy structure ('Minimum', top), in a flat orientation ('Flat', middle) as well as in an asymmetric proton transfer situation ('Asymm', bottom) centered in a truncated octahedron periodic supercell hosting in addition 88 He atoms. Black, solid: Energies obtained from the coupled cluster grid. Red, dotted: NNP evaluated at the coupled cluster grid points.

figuration with asymmetric proton sharing that featured the largest deviations upon microsolvation, most VADs obtained on both grids are in very good agreement. However the shallower region around the excess proton of the NNP compared to the reference grid again causes slight shifts in the VAD locations. Since their number and also shape is still correctly reproduced and the RDFs are in very good agreement, the solvation of the Zundel cation

by bulk helium is expected to be described with very high accuracy by the NNP.

IV. CONCLUSIONS AND OUTLOOK

In conclusion, we have presented a systematic and largely automated procedure to develop pairwise additive He-solute interaction potentials employing high-dimensional neural networks. This NNP approach yields very convincing agreement with the high level reference electronic structure method being CCSD(T) in an essentially converged basis set in the present cases, being the protonated water monomer and dimer. The flexibility of the NNs allows to easily identify deficiencies in the training set which can be used to systematically improve the NNP while substantially reducing the number of expensive reference calculations. This opens the door for fast and accurate development of He-solute interaction potentials and therefore overcomes the obstacles of traditional fitting approaches used so far in this field. For the chosen solutes in this study, i.e. H_3O^+ and H_5O_2^+ , we were able to correctly describe the solvation structure upon stepwise microsolvation with helium – from one adatom up to the solvation in bulk helium with the same accuracy. This enables the study of the solvation of these clusters by superfluid helium all the way from a few helium atoms to the bulk superfluid. In addition, the presented procedure will open the door to study other solute species solvated by quantum fluids including parahydrogen, $p\text{-H}_2$, and therefore will provide new insights into the nature of fundamental inter- and intramolecular interactions in quantum solvation.

SUPPLEMENTARY MATERIAL

See the supplementary material for additional validations of the computational methods, details on the symmetry function setup and the comprehensive set of all spatial distribution functions.

ACKNOWLEDGMENTS

It gives us great pleasure to thank Harald Forbert for helpful discussions. This research is part of the Cluster of Excellence "RESOLV" (EXC 1069) funded by the *Deutsche Forschungsgemeinschaft*, DFG. J.B. thanks the DFG for a Heisenberg Professorship (Be3264/11-1) and C.S. acknowledges partial financial support from the *Stiftung des Deutschen Volkes* as well as the *Verband der Chemischen Industrie*. The computational resources were provided by HPC@ZEMOS, HPC-RESOLV, BOVI-LAB@RUB, and RV-NRW.

REFERENCES

- ¹J. P. Toennies and A. F. Vilesov, *Annu. Rev. Phys. Chem.* **49**, 1 (1998).
- ²J. P. Toennies and A. F. Vilesov, *Angew. Chemie Int. Ed.* **43**, 2622 (2004).
- ³J. P. Toennies, *Mol. Phys.* **111**, 1879 (2013).
- ⁴S. Goyal, D. L. Schutt, and G. Scoles, *Phys. Rev. Lett.* **69**, 933 (1992).
- ⁵D. M. Ceperley, *Rev. Mod. Phys.* **67**, 279 (1995).
- ⁶P. Sindzingre, M. L. Klein, and D. M. Ceperley, *Phys. Rev. Lett.* **63**, 1601 (1989).
- ⁷S. Grebenev, J. P. Toennies, and A. F. Vilesov, *Science* **279**, 2083 (1998).
- ⁸R. A. Aziz, V. P. S. Nain, J. S. Carley, W. L. Taylor, and G. T. McConville, *J. Chem. Phys.* **70**, 4330 (1979).
- ⁹K. Szalewicz, *Int. Rev. Phys. Chem.* **27**, 273 (2008).
- ¹⁰D. Kuchenbecker, F. Uhl, H. Forbert, G. Jansen, and D. Marx, *Phys. Chem. Chem. Phys.* **19**, 8307 (2017).
- ¹¹L. Walewski, H. Forbert, and D. Marx, *Comput. Phys. Commun.* **185**, 884 (2014).
- ¹²L. Walewski, H. Forbert, and D. Marx, *J. Chem. Phys.* **140**, 144305 (2014).
- ¹³A. D. Boese, H. Forbert, M. Masia, A. Tekin, D. Marx, and G. Jansen, *Phys. Chem. Chem. Phys.* **13**, 14550 (2011).
- ¹⁴J. Behler and M. Parrinello, *Phys. Rev. Lett.* **98**, 146401 (2007).
- ¹⁵J. Behler, *Phys. Chem. Chem. Phys.* **13**, 17930 (2011).
- ¹⁶J. Behler, *J. Phys. Condens. Matter* **26**, 183001 (2014).
- ¹⁷J. Behler, *Int. J. Quantum Chem.* **115**, 1032 (2015).
- ¹⁸J. Behler, *J. Chem. Phys.* **145**, 170901 (2016).
- ¹⁹J. Behler, *Angew. Chemie Int. Ed.*, 10.1002/anie.201703114 (2017).
- ²⁰T. Morawietz, A. Singraber, C. Dellago, and J. Behler, *Proc. Natl. Acad. Sci.* **113**, 8368 (2016).
- ²¹B. Cheng, J. Behler, and M. Ceriotti, *J. Phys. Chem. Lett.* **7**, 2210 (2016).
- ²²V. Kapil, J. Behler, and M. Ceriotti, *J. Chem. Phys.* **145**, 234103 (2016).
- ²³M. Hellström and J. Behler, *Phys. Chem. Chem. Phys.* **19**, 82 (2016).
- ²⁴M. Hellström and J. Behler, *J. Phys. Chem. B* **121**, 4184 (2017).
- ²⁵S. K. Natarajan and J. Behler, *Phys. Chem. Chem. Phys.* **18**, 28704 (2016).
- ²⁶V. Quaranta, M. Hellström, and J. Behler, *J. Phys. Chem. Lett.* **8**, 1476 (2017).
- ²⁷D. Marx and J. Hutter, *Ab Initio Molecular Dynamics: Basic Theory and Advanced Methods* (Cambridge University Press, Cambridge, 2009).
- ²⁸“CP2K, freely available at the URL <http://www.cp2k.org>, released under GPL license.”
- ²⁹J. Hutter, M. Iannuzzi, F. Schiffmann, and J. VandeVondele, *Wiley Interdiscip. Rev. Comput. Mol. Sci.* **4**, 15 (2014).
- ³⁰J. VandeVondele, M. Krack, F. Mohamed, M. Parrinello, T. Chassaing, and J. Hutter, *Comput. Phys. Commun.* **167**, 103 (2005).
- ³¹B. Hammer, L. B. Hansen, and J. K. Nørskov, *Phys. Rev. B* **59**, 7413 (1999).
- ³²S. Grimme, J. Antony, S. Ehrlich, and H. Krieg, *J. Chem. Phys.* **132**, 154104 (2010).
- ³³S. Goedecker, M. Teter, and J. Hutter, *Phys. Rev. B* **54**, 1703 (1996).
- ³⁴T. Morawietz and J. Behler, *J. Phys. Chem. A* **117**, 7356 (2013).
- ³⁵K. Forster-Tonigold and A. Groß, *J. Chem. Phys.* **141**, 064501 (2014).
- ³⁶M. Ceriotti and D. E. Manolopoulos, *Phys. Rev. Lett.* **109**, 100604 (2012).
- ³⁷F. Uhl, D. Marx, and M. Ceriotti, *J. Chem. Phys.* **145**, 054101 (2016).
- ³⁸R. A. Kendall, T. H. J. Dunning, and R. J. Harrison, *J. Chem. Phys.* **96**, 6796 (1992).
- ³⁹D. E. Woon and T. H. Dunning Jr., *J. Chem. Phys.* **100**, 2975 (1994).
- ⁴⁰S. F. Boys and F. Bernardi, *Mol. Phys.* **19**, 553 (1970).
- ⁴¹H.-J. Werner, P. J. Knowles, G. Knizia, F. R. Manby, M. Schütz, and Others, *MOLPRO, version 2012.1, a package of ab initio programs* (molpro, 2012).
- ⁴²J. Behler, *J. Chem. Phys.* **134**, 074106 (2011).
- ⁴³S. Shah, F. Palmieri, and M. Datum, *Neural Networks* **5**, 779 (1992).
- ⁴⁴T. B. Blank and S. D. Brown, *J. Chemom.* **8**, 391 (1994).
- ⁴⁵J. B. Witkoskie and D. J. Doren, *J. Chem. Theory Comput.* **1**, 14 (2005).
- ⁴⁶J. Behler, “RuNNer - A Neural Network Code for High-Dimensional Potential-Energy Surfaces.”
- ⁴⁷L. J. LaBerge and J. C. Tully, *Chem. Phys.* **260**, 183 (2000).
- ⁴⁸C. W. Murray, N. C. Handy, and G. J. Laming, *Mol. Phys.* **78**, 997 (1993).
- ⁴⁹V. I. Lebedev, *Sib. Math. J.* **18**, 99 (1977).
- ⁵⁰M. Tuckerman, *Statistical Mechanics: Theory and Molecular Simulation*, Oxford Graduate Texts (OUP Oxford, 2010).
- ⁵¹R. N. Barnett and K. B. Whaley, *J. Chem. Phys.* **99**, 9730 (1993).
- ⁵²Y. Kwon, D. M. Ceperley, and K. B. Whaley, *J. Chem. Phys.* **104**, 2341 (1996).
- ⁵³Y. Kwon, P. Huang, M. V. Patel, D. Blume, and K. B. Whaley, *J. Chem. Phys.* **113**, 6469 (2000).
- ⁵⁴C. D. Paola, E. Bodo, and F. A. Gianturco, *Eur. Phys. J. D - At. Mol. Opt. Plasma Phys.* **40**, 377 (2006).
- ⁵⁵E. Coccia, E. Bodo, F. Marinetti, F. A. Gianturco, E. Yildirim, M. Yurtsever, and E. Yurtsever, *J. Chem. Phys.* **126**, 124319 (2007).
- ⁵⁶D. E. Galli, D. M. Ceperley, and L. Reatto, *J. Phys. Chem. A* **115**, 7300 (2011).